EurJIC
European Journal of Inorganic Chemistry

Research Article
doi.org/10.1002/ejic.202200078

Chemistry Europe
European Chemical Societies Publishing

www.eurjic.org

Low-Coordinated Iron(II) Siloxide Complexes – Structural Diversity and Reactivity Towards O_2 and Oxygen Atom Transfer Reagents

Stefan Yelin,[a] Beatrice Cula,[a] and Christian Limberg*[a]

The coordination chemistry of Fe^{2+} ions in combination with a monodentate siloxide ligand Ph_3SiO^- (L) was investigated. Using a Fe/L stoichiometry of 1:3 the complex [Na(DME)][FeL_3], **2**, with the iron center in a trigonal ligand environment was isolated and through decreasing the siloxide amount fraction **2** was shown to form via a unique example of a dinuclear complex, where one of the iron ions has a quasi-trigonal and the other one a tetrahedral coordination sphere, namely [Na(DME)][Fe_2L_5], **1**. If, however, 4 equivalents of L are employed, the tetrasiloxido ferrate(II) anion with a tetrahedral structure is generated, so that the product [Na(DME)]$_2$[FeL_4], **3**, can be isolated. **2** reacts instantly with O-atom transfer reagents, also at low temperatures, but no reaction intermediate could be identified. From the product mixture the iron(III) siloxide complex [Na(DME)$_3$][FeL_4], **4**, could isolated by crystallization as the main product. Likewise, the reaction with dioxygen proceeded rather fast and added substrates did not intercept any intermediate upon its formation. However, in the presence of cyclohexene oxidation products were observed. They correspond to the typical radical-chain-derived products of cyclohexene suggesting, that initially a reactive FeO_x species is generated that via an H atom abstraction from cyclohexene triggers its autoxidation.

Introduction

Through treatment of silica or silicate materials with iron precursors rather interesting materials can result, some of which have proved potent heterogeneous catalysts for the oxidation of hydrocarbons.[1,2] The most prominent examples are the catalysts produced originally by Panov and coworkers[3] which were shown only recently to contain iron centers in square planar coordination spheres with high-spin configuration (α-Fe sites).[4,5] They have proved capable of reacting with O-atom transfer (OAT) reagents such as N_2O to give highly reactive Fe^{IV}=O sites that can oxygenate methane and benzene. However, also other coordination environments that silica surfaces can provide for iron centers lead to reactive sites. For instance, Tilley and coworkers have shown that grafting of the iron(III) siloxide [Fe(OSi(OtBu)$_3$)$_3$(THF)] on SBA-15 leads to isolated iron(III) sites, and after calcination the material represents a highly selective oxidation catalyst.[6]

Silanols are often regarded as low-molecular-weight analogues for hydroxylated silica surfaces as they possess both structural and electronic similarities. In turn, their reactions with transition-metal precursors thus mimic the impregnation processes applied for the preparation of heterogeneous catalysts, and the resulting metal siloxides can provide information about what kind of reactivities can be expected for certain structural units suspected to occur on the surfaces of heterogeneous catalysts;[7] obviously establishing such reactivity in homogeneous liquid phase is an attractive goal. If we thus shift the focus to molecular iron siloxide compounds it is noted that their number is still quite limited and investigations on their reactivity are rare.[2]

With this background we have developed an interest in the chemistry of iron siloxide chemistry and in recent years accessed various high-spin square planar representatives, which served as structural and spectroscopic models for the above-mentioned α-Fe sites.[8–11] Investigating their reactivity, they were found to behave inert toward oxygen atom transfer reagents but extremely reactive towards O_2.

Here we start to turn our attention also to other structural motifs, and one that appears particularly interesting is the trigonal planar siloxide coordination of iron(II) centers, as the resulting rather weak ligand field promises the formation of highly reactive species (e.g. Fe^{IV}=O complexes) in contact with oxygenating reagents.[12,13] In 2013 Nocera and coworkers have shown that an iron(II) alkoxide with a trigonal planar structure, namely [Fe(ditox)$_3$][K(15-crown-5-ether)$_2$] (ditox = ^{t}Bu$_2$(Me)CO$^-$) is capable of reacting with OAT reagents, such as PhIO and Me_3NO, and the resulting products rapidly oxygenated C–H bonds belonging to the solvent.[13] An Fe^{IV}=O was proposed to form in the initial OAT reaction, which can be intercepted in some solvents to oxidize phosphines to phosphine oxide.

[a] S. Yelin, Dr. B. Cula, Prof. Dr. C. Limberg
Institut für Chemie, Humboldt-Universität zu Berlin
Brook-Taylor-Straße 2 12489 Berlin, Germany
E-mail: christian.limberg@chemie.hu-berlin.de
http://www.chemie.hu-berlin.de/aglimberg

Supporting information for this article is available on the WWW under https://doi.org/10.1002/ejic.202200078

Research Article
doi.org/10.1002/ejic.202200078

Combining this information on Fe-zeolites/silicates and on iron siloxides/alkoxides, studies on tri(siloxido)ferrate(II) compounds suggest themselves. Only few representatives of this compound class are known so far and their behavior is hardly explored.[2] For instance, $[((Me_3Si)_3SiO)_3Fe]Na(DME)$ has been described in 1997 but its reactivity was not investigated.[14]

In the following we describe the results obtained investigating the reactivity of iron(II) siloxides with different coordination spheres towards OAT reagents and O_2.

Results and Discussion

Complex formation. The siloxide ligand Ph_3SiO^- (L) was chosen and it was introduced at the iron(II) centers through salt metathesis reactions. Hence, LH was deprotonated with NaH and the resulting sodium salt (LNa) was reacted with $FeBr_2$, first of all in the ratio 2.5:1, resulting in the formation of the dinuclear complex $[Na(DME)][Fe_2L_5]$, **1**. The reaction of LNa with $FeBr_2$ in the ratio of 3:1 resulted in the formation of the mononuclear complex $[Na(DME)][FeL_3]$, **2**, while the complex $[Na(DME)]_2[FeL_4]$, **3**, was obtained by reacting LNa with $FeBr_2$ in the ratio 4:1. Crystals of good quality could be grown by layering saturated toluene solutions of **1**, **2** or **3** with *n*-hexane (Scheme 1).

Compared to bidentate disilanolate ligands such as $[O(SiPh_2O)_2]^{2-}$ the monodentate silanolate ligand Ph_3SiO^- thus enables the selective synthesis of complexes varying with regards to coordination spheres around the iron(II) ions as well the nuclearity, solely based on the ratio of ligand to iron precursor. Complex **1** crystallizes in form of reddish-brown needles, that is, with a color clearly different from the one displayed by the abovementioned mono- and dinuclear iron(II) siloxides with high-spin square planar FeO_4 centers, which are colored in shades of blue.[9–11] This may be the result of the unusual combination of the two iron centers with different connectivities in **1** (see discussion below). Complex **2** forms pale blueish-green needles. The pale color arises from forbidden d-d transitions with a low intensity absorption maximum at $\lambda =$ 770 nm. Complex **3** crystallizes as pale green blocks, and its UV/Vis spectrum features a low intensity absorption maximum only slightly redshifted (as compared to **2**) to $\lambda = 785$ nm.

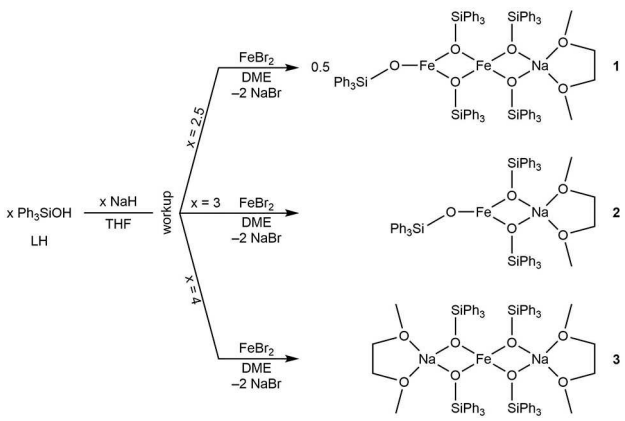

Scheme 1. Synthesis of complexes **1**, **2** and **3**.

Given the increase of the stoichiometry of L within the series of compounds **1**–**3** it is highly likely, that the synthesis of **3** with the highest content of L proceeds via compounds **1** and **2**. This hypothesis is supported by a color change of the initial reaction solution from brown via blueish-green to green in the synthesis of **3**.

Complex **1** probably is formed via initial generation of complex Fe_2L_4 with a 1:2 stoichiometry (compare $[Fe_2(OSi(O^tBu)_3)_4]$[15]) through reaction with one equivalent of LNa and it then reacts in a further step with another equivalent of LNa yielding two equivalents of complex **2**. In a final step complex **2** reacts with another equivalent of LNa to form **3**. An investigation of the product mixture isolated after the reaction of $FeBr_2$ with 3.1 equivalents of LNa with Mössbauer spectroscopy further supports this theory by revealing a major species corresponding to **2** and a minor species corresponding to **3** (Figure S19, Mössbauer data of all complexes will be discussed in more detail below). Therefore, **1** and **2** can be seen as snapshots in the synthesis of **3**.

Structural properties. The iron(II) centers in the dinuclear complex **1** exhibit different connectivities and are connected by two bridging silanolate ligands (Figure 1). The Fe2 iron center is coordinated by three siloxide ligands with Fe–O bond lengths of 1.949(1) Å and 1.917(1) Å found for the two bridging O atoms and 1.823(2) Å for the terminal ligand. The angles O1–Fe2–O3 135.65(6)°, O2–Fe2–O3 135.28(7)° and O1–Fe2–O2 89.04(5)° add up to 360° thus confirming a perfectly planar Y-shaped coordination. The Fe1 iron center is surrounded by four ligands with a τ_4 value of 0.81 indicating a distorted tetrahedral coordination sphere. The Fe1–O bonds belonging to silanolates bridging to Fe2 are 2.071(1) Å and 2.119(1) Å, the other two from bridges to a sodium cation, which itself is additionally coordinated by a DME solvent molecule, with Fe–O bond lengths of 1.901(1) Å and 1.913(1) Å. The Fe2–O1/2 bonds are notably shorter as compared to the Fe1–O1/2 bonds, which will be a result of the lower coordination number of Fe1. The distance between both iron centers is 2.9760(9) Å. Complex **1** represents, to the best of our knowledge, the first example of a dinuclear iron(II) complex with both a quasi-trigonal and a tetrahedral coordination sphere.

As Fe2 in **1**, the iron(II) ion in the mononuclear complex **2** is coordinated by three ligands. The sum of the three O–Fe–O angles in **2** amounts to 360° and thus confirms the perfect planar Y-shaped coordination. A sodium cation is coordinated by two of the silanolate O atoms and a DME solvent molecule. The comparison of the two angles O1–Fe2–O2 89.04(5)° in **1** and O2–Fe1–O1 98.1(3)° in **2** shows that the Y-shaped coordination in **2** is closer to trigonal planar than the respective coordination sphere in **1**. Viewing the metal-siloxide contacts as Lewis acid/base interactions, this can be rationalized as follows: Starting from a trigonal planar $[FeL_3]^-$ moiety (involving Fe2 in **1** and Fe1 in **2**), the Fe1 ion in **1** more effectively competes for electron density and coordination than the sodium ion in **2**; hence in **1** O1 and O2 are slightly pulled away from the central iron center (Fe2–O1 1.949(1), Fe2–O2 1.917(1) vs. Fe2–O3

Research Article
doi.org/10.1002/ejic.202200078

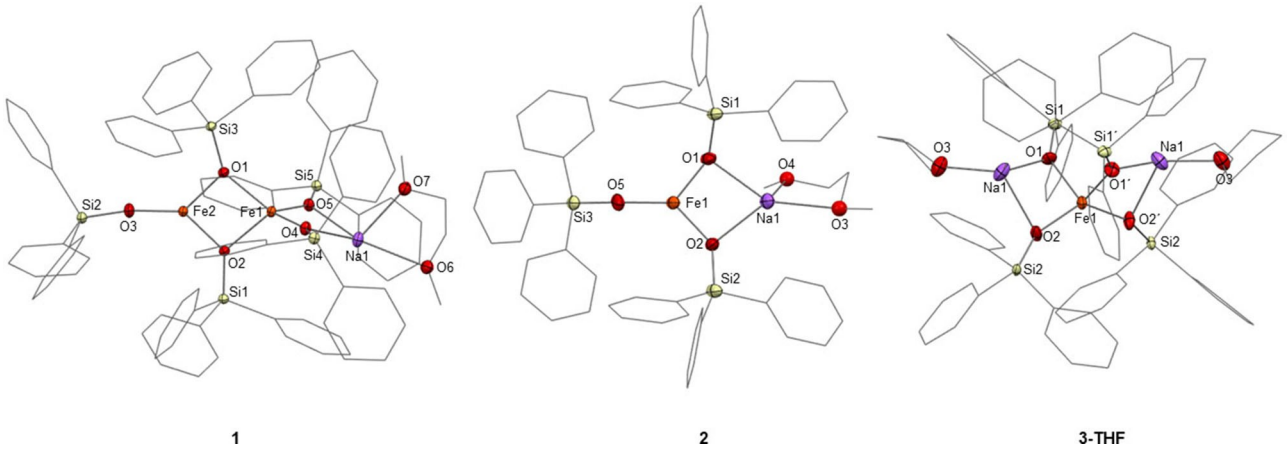

Figure 1. Molecular structures of **1**, **2** and **3-THF**, as determined by single-crystal XRD. Hydrogen atoms and non-coordinating solvent molecules are omitted for clarity. Selected bond lengths [Å] and angles [°]: **1**: Fe1–O5 1.913(1), –O4 1.901(1), –O1 2.071(1), –O2 2.119(2), Fe2–O1 1.949(1), –O2 1.917(1), –O3 1.823(2). O1–Fe2–O3 135.65(6), O1–Fe2–O2 89.04(5), O2–Fe2–O3 135.28(7), O2–Fe1–O1 80.62(5), O5–Fe1–O2 117.47(6), O1–Fe1–O4 118.81(5), O4–Fe1–O5 101.36(5). **2**: Fe1–O1 1.912(6), –O2 1.887(5), –O5 1.851(7), O2–Fe1–O1 98.1(3), O5–Fe1–O2 128.0(3), O1–Fe1–O5 133.9(3). **3-THF**: Fe1–O1 2.017, –O2 1.926, O1–Fe1–O1' 98.32, O2–Fe1–O1 95.02, O2–Fe1–O2' 129.02.

1.823(2) Å) and the O2–Fe2–O1 angle is decreased (89.04(5)°), while in **2** the contact with Na1 leads to less distortion (Fe1–O1 1.912(6), –O2 1.887(5), –O5 1.851(7), O2–Fe1–O1 98.1(3)°).

The successful synthesis of **3** could be confirmed by Mössbauer spectroscopy, elemental analysis and ESI-MS studies. Numerous different crystallization methods only yielded disordered crystals of **3**, though, not suitable for X-ray crystal structure analysis, and therefore the structure generated and crystal data are not shown in Figure 1. However, crystals of adequate quality could be grown for the THF analogon of **3**, namely **3-THF**, obtained after performing the synthesis in THF instead of DME. The iron center of **3-THF** is surrounded by four silanolate ligands and a τ_4 value of 0.83 shows, that the coordination sphere is close to tetrahedral. The Fe1–O1/1′ bond length amounts to 2.017(2) Å, while the Fe1–O2/2′ bonds are with 1.926(2) Å significantly shorter. Two sodium cations are each coordinated by two bridging siloxide O atoms and a THF solvent molecule.

Mössbauer spectroscopic investigations. Subsequently, all complexes were investigated by Mössbauer spectroscopy to clarify spin states and the impact of different coordination spheres on the isomer shifts (δ) and quadrupole splittings (ΔE_Q); the corresponding values are listed in Table 1.

As expected, the structural diversity of the four complexes is reflected in the Mössbauer values. Their isomer shifts range between 0.77 and 1.16 mm/s, corresponding to iron(II) in a high spin state. This result is in line with the expectations, as siloxide ligands generate a weak ligand field, favoring a high spin state of the metal center.[10] The Mössbauer spectrum of **1** (Figure 2 and Figure S17) contains two signals in a 1/1 ratio. Interestingly, the isomer shift of the three-coordinated iron center (δ = 0.77 mm/s) is small in comparison to the isomer shift of the four coordinated iron(II) (δ = 1.04 mm/s). This can be explained with the shorter Fe–O bond lengths characterizing the three coordinated iron.[16] As the isomer shift arises from an electric monopole coulomb interaction between the electron density at the nucleus (s orbitals) and the nuclear charge, any deviation in s orbital density at the nucleus causes a change in resonance

Table 1. Mössbauer data of complexes **1**, **2**, **3** and **3-THF**.

	1[a]		**2**	**3**	**3-THF**
	Fe^3	Fe^4			
δ [mm/s]	0.77	1.04	0.74	1.16	1.13
ΔE_Q [mm/s]	1.02	2.40	0.95	2.66	2.51

[a] The exponent indicates the coordination number.

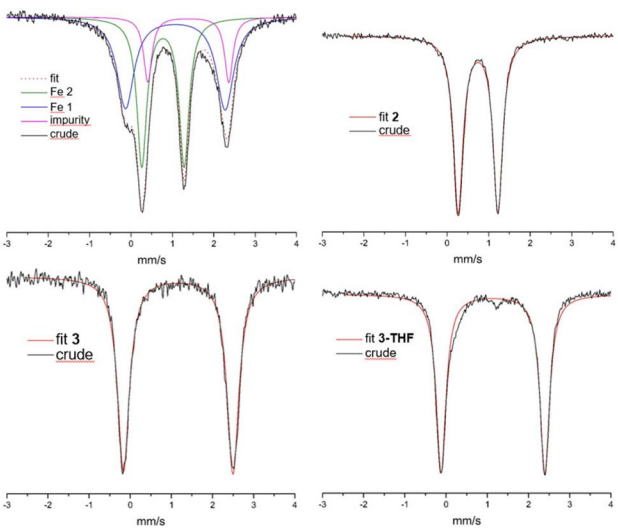

Figure 2. Mössbauer spectra of **1**–**3** at 15 K (black lines) and fittings (red dots/lines). In case of **1** (top left) also the deconvolution into subspectra is shown, including an unknown impurity with < 8% (δ [mm/s] = 1.38, ΔE_Q [mm/s] = 1.95).

Research Article
doi.org/10.1002/ejic.202200078

energy with the source. Shorter bonds lead to a compression of the 3 s- and 4 s-iron orbitals thus increasing the electron density at the nucleus and lowering the isomer shift. The quadrupole splittings observed for the iron centers with Y-shaped coordination are with $\Delta E_Q = 1.02$ mm/s (**1**) and $\Delta E_Q = 0.95$ mm/s (**2**) comparably small for iron(II) high-spin complexes, however they are line with literature.[17,18] The small ΔE_Q values can be explained with the negative electric field gradient (EFG) arising from the asymmetric electron distribution being compensated by a ligand contribution, which in planar complexes provides a large positive EFG component perpendicular to the ligand plane.[17] For high-spin iron(II) ions in tetrahedral coordination spheres ΔE_Q values of 2.40 mm/s (**1**) and 2.66 mm/s (**3**) are quite typical, while for square planar coordination rather small values are characteristic, as the electric field gradient caused by the single β electron in the dz^2 orbital is compensated by the lattice contribution arising by the square planar ligand field (opposite sign).[19]

Reactivity towards oxidants. Inspired by the work of Nocera *et al.* on iron(II) high-spin complexes in a trisalkoxide ligand environment, we finally examined the reactivity of **2** towards oxidizing agents. As Fe^{IV}=O species are considered to play a central role in the catalytic cycles of heme and non-heme iron in enzymes[20] and also in the reactivity of synthetic catalysts (e.g. in the Panov system[4]) we attempted to generate such units starting from **2** using the OAT reagents soluble-iodosobenzene (^{s}PhIO), trimethylamine-*N*-oxide and pyridine-*N*-oxide for reactivity studies. These two-electron oxidizing agents, were envisaged to give direct access to a highly reactive Fe^{IV}=O species starting from an iron(II) complex. However, reactions of **2** with these OAT reagents occur rather rapidly and are instantly finished at r.t., as indicated by a color change of the solution from blueish-green to yellow-brown, and no intermediate could be observed, even at temperatures as low as −125 °C using 2-methyltetrahydrofuran as a solvent. The extreme sensitivity of **2** towards OAT reagents is at first sight surprising, as in our previous studies on a high-spin square planar iron(II) siloxide complex, namely $[Li(THF)_2]_2[Fe(O(SiPh_2O)_2)_2]$, **I**, no reactivity, even at temperatures up to 80 °C, was observed.[11] This may be attributed to the fact that **2** is lacking one ligand in comparison, so that the sterics are more favorable and furthermore it has a lower charge. In an attempt to isolate oxidation products of **2**, one equivalent of trimethylamine-*N*-oxide was added to a pale blueish-green solution of **2** in toluene. The solution turned brown in an instant, and a colorless precipitate started to form after ~30 seconds. Out of this reaction mixture complex $[Na(DME)_3][FeL_4]$, **4**, was isolated by crystallization.

The iron(III) center in **4** (Figure 3) is tetrahedrally coordinated by four ligands. A sodium counter ion is coordinated by three dimethoxyethane solvent molecules in a slightly distorted octahedral fashion. Formation of a one-electron oxidized version of **2** is rather surprising, as Me_3NO is expected to transfer an O atom in the initial step to give a Fe^{IV}=O complex, and such species then typically react further via C–H bond activation to yield an Fe(III)–OH product, like in case of the ditox system investigated by Nocera. However, also after multiple attempts under different reaction conditions, such as

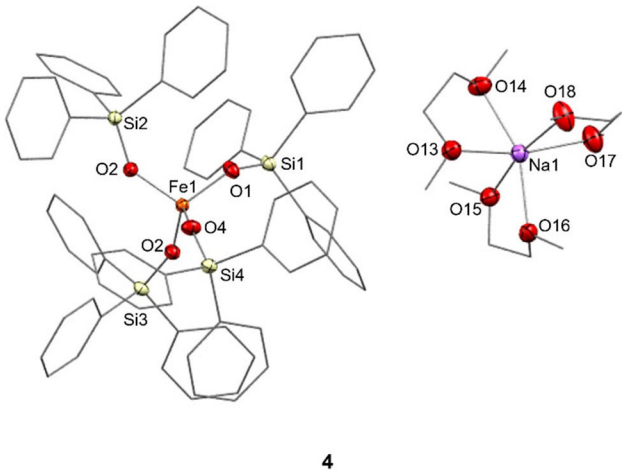

4

Figure 3. Molecular structure of **4** as determined by single-crystal XRD. Hydrogen atoms and non-coordinating solvent molecules are omitted for clarity. Selected bond lengths [Å] and angles [°]: Fe1–O1: 1.850(2), –O2: 1.846(2), –O3 1.855(2), –O4 1.849(2); O1–Fe1–O2 111.22(9)°, O2–Fe1–O3 109.44(9)°, O3–Fe1–O4 109.72(9)°, O1–Fe1–O4 109.98(9)°.

low temperatures and with different solvents, no such compound could be isolated by crystallization. Despite that, Mössbauer measurements performed with the product mixture isolated after the reaction of **2** with Me_3NO revealed the existence of two different iron(III) species (Figure S18). Their isomeric shifts of $\delta = 0.34$ mm/s and 0.35 mm/s indicate that they both contain iron(III) ions in high-spin states. One signal (66%) shows a small quadrupole splitting of $\Delta E_Q = 0.44$ mm/s that indicates a rather symmetric environment and fits to a tetrahedral coordination of the iron center,[19] while the second signal (33%) with $\Delta E_Q = 0.98$ mm/s suggests a somewhat more asymmetric ligand sphere and may belong to a high-spin iron(III) complex with a coordination number of five or six.[19] As work-up of the reaction mixture has led to the isolation of complex **4**, the structure of which is in line with the requirements of the major signal, it is reasonable to assign it **4**. Thus the second, structurally unknown, product might contain one or more Fe(III)–OH moieties. An IR spectrum recorded of the reaction mixture (KBr disk) indeed revealed a low intensity sharp band at $\nu = 3648$ cm^{-1}, which may support the formation of an Fe(III)–OH product.[13] In further studies, the reaction was repeated in toluene-d_8 to clarify the origin of the H atom. However, no shift of the band could be observed. This leads us to the conclusion, that a potentially formed Fe^{IV}=O intermediate rather abstracts an H atom from a ligand phenyl group, than from the solvent.

To test for in-situ oxygenation reactivity, different molecules such as triphenylphosphine, thioanisole and cyclohexene, where employed that are known to function as acceptors for O atoms derived from Fe^{IV}=O oxidants.[13,21–23] However, even after using inert solvents like 1,2-fluorobenzene and hexafluorobenzene, to exclude a side reaction with the solvent, no oxidized compounds such as triphenylphosphine oxide, methylphenyl sulfoxide or cyclohexene oxide could be detected. This is consistent with the aforementioned assumption, that the

Research Article
doi.org/10.1002/ejic.202200078

reactive intermediate immediately reacts with a ligand phenyl group in close proximity, prohibiting a reaction with a substrate molecule. These findings show the benefits and disadvantages of a monopodal ligand system. On one side a monopodal ligand allows for the synthesis of highly reactive complexes like **2** by creating an iron(II) moiety that is sterically accessible for Me_3NO and has a low charge, on the other hand, a dipodal ligand system makes the complex and its reaction products more stable. This is also reflected in the NO reactivity: both **2** and the DME analogue of **I**, **I-DME**, immediately react with NO resulting in purple solutions. In the case of **I-DME** a NO complex could be isolated by crystallization,[11] while the purple solution of **2** with NO turned brown in ~30 min and it was not possible to isolate a NO complex.

After investigating the behavior of **2** towards OAT reagents, the focus was shifted towards the activation of dioxygen, to clarify whether any reactive species could be intercepted (using the compounds already employed while investigating the reaction of **2** with OAT reagents). However, only in the case of cyclohexene an oxidation reaction could be confirmed by gas chromatography coupled to mass spectrometry (GC MS) and nuclear magnetic resonance (NMR) studies. For this, compound **2** was dissolved in cyclohexene and O_2 was bubbled through the solution for 20 s. Immediately, the pale blueish-green solution turned yellow and the reaction was stirred at room temperature for 16 h. The formation of four oxidation products, namely cyclohexene oxide, 2-cyclohexene-1-ol, 2-cyclohexene-1-one and 7-oxabicyclo[4.1.0]heptan-2-one (Scheme 2), was confirmed by GC MS in a ratio of 1:7:1:6 (GC MS; TON = 10.5), indicating that autoxidation has occurred.

Indeed, the oxygenation of cyclohexene can take two possible reaction pathways. Either epoxidation takes place, that is, cyclohexene is directly oxidized to cyclohexene oxide, which is the usual pathway observed for Fe^{IV}=O species,[22] or a radical chain reaction is initiated. In the latter, the reactive intermediate resulting from the reaction between the iron(II) complex and dioxygen abstracts an H atom resulting in the formation of a cyclohexenyl radical, which reacts to 2-cyclohexene-1-hydroperoxide (C–OOH). This can react with another cyclohexene molecule to form cyclohexene oxide or decompose into 2-cyclohexene-1-ol and 2-cyclohexene-1-one.[24,25] Hence the product spectrum mentioned above is indicative of an autoxidation path. Proceeding of the reaction via a radical chain route was further supported by the observation of a fifth oxidation product in GC MS measurements with a mass spectrum strongly resembling a mass spectrum recently published by Wei *et al.*, which was assigned to cyclohexene-1-hydroperoxide.[25] Assignment of this signal to a C–OOH product was further underpinned by adding triphenylphosphine, PPh_3, to a sample of the oxidation products: C–OOH compounds are known to react with PPh_3 to give triphenylphosphine oxide, PPh_3O, and 2-cyclohexen-1-ol.[26] After the addition of PPh_3 the sample was analyzed again by GC MS, revealing the disappearance of the C–OOH peak. At the same time, as expected, the peak area of 2-cyclohexen-1-ol increased concomitantly, whereby the peak areas of the remaining oxidation products remained unchanged. The formation of PPh_3O was confirmed by GC MS and ^{31}P NMR spectroscopic studies (Supporting Information). Further evidence for the radical chain mechanism and thus also for the formation of C–OOH, is the formation of 7-oxabicyclo[4.1.0]heptan-2-one, as recent studies showed, that a reaction between 2-cyclohexene-1-hydroperoxide and 2-cyclohexene-1-on leads to the formation of 7-oxabicyclo[4.1.0]heptan-2-one.[27] Finally, to prove, that the oxygen atoms in the products are derived from O_2, experiments with $^{18}O_2$ were performed. Indeed, GC MS studies showed, that, when employing $^{18}O_2$, the detected masses shift by two m/z, respectively, four in the case of 7-oxabicyclo[4.1.0]heptan-2-one (Figure 4). Additionally, blank tests in the absence of **2** showed no oxidation of cyclohexene, even not when $FeBr_2$ or $Fe(OAc)_2$ were present instead.

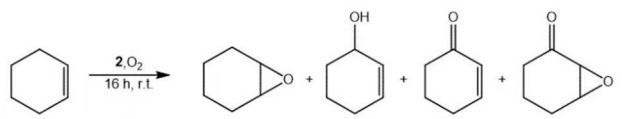

Scheme 2. Oxidation of cyclohexene with **2**.

Conclusions

Silicate-supported iron centers have proven catalytically active in oxygenation reactions. To a certain extent siloxide ligands can simulate the surroundings which iron ions experience on such silicate surfaces and – especially with low-coordination numbers – they generate a weak ligand field that upon contact of iron siloxides with oxygenating reagents should lead to rather reactive FeO_x species. With this background the synthesis of iron(II) siloxido compounds was studied to test their reactivity towards oxidants. Using triphenylsilanolate (L) as a ligand it was found that it is possible to successively construct iron(II) silanolates with varying Fe/L stoichiometries in a controlled fashion. One of them, **1**, features a unique structural motif, namely a dinuclear core, where one of the iron ions has a quasi-trigonal coordination sphere while the second one is coordinated tetrahedrally. The behaviour of the tricoordinated representative **2** in contact with OAT reagents was tested and as anticipated a rather high reactivity was found even at low temperature. This exceptionally high reactivity prohibited the identification of an intermediate or even the interception of such by addition of oxidizable substrates. One of the products was identified as the one-electron oxidized version of **2**, **4**, and Mössbauer spectroscopic investigations revealed the formation of a second iron(III) product that may contain the O atom of the reagents in form of a hydroxide group. Reaction of **2** with O_2 proceeded instantaneously, too, and when the reaction was carried out in neat cyclohexene, radical-chain-derived oxidation products of cyclohexene were found suggesting, that initially a reactive FeO_x species is generated that via an H atom abstraction from cyclohexene triggers its autoxidation. Altogether, therefore, low-coordinated iron(II) siloxide complexes and the species formed upon contact with oxidants exhibit the

Research Article
doi.org/10.1002/ejic.202200078

Chemistry Europe
European Chemical Societies Publishing

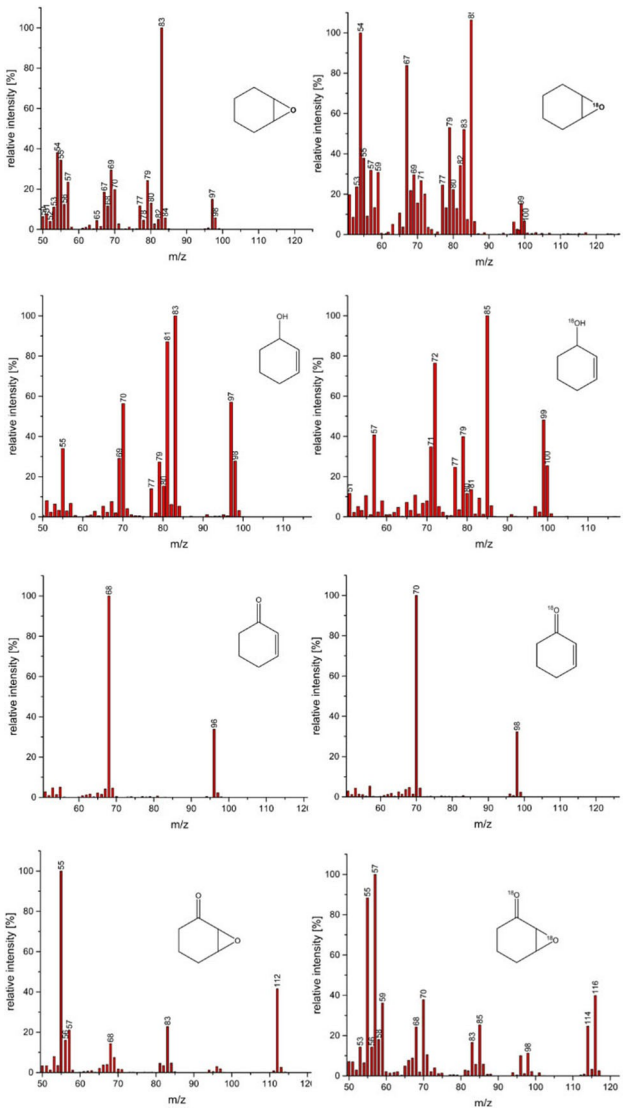

Figure 4. GC/MS data of the products formed in the reaction of **2** dissolved in cyclohexene for 16 h at room temperature and ambient pressure with $^{16}O_2$ and $^{18}O_2$, respectively. The m/e values observed after the $^{18}O_2$ reaction reveal that O_2 is the source of oxygen in the products of this catalytic reaction. Employing the same reaction conditions but in the absence of **2**, no such reaction products could be detected with either GC/MS, GC/FID or NMR. Even when $FeBr_2$ or $Fe(OAc)_2$ where added instead of **2** no oxidation products could be observed.

envisaged high reactivity. The latter, however, also represents a limitation of the system since the surroundings (ligand substituents) instead of substrates are attacked. Future work will thus focus on appropriate variations of the substituents at the Si atoms.

Experimental Section

Materials: Sodium hydride, triphenyl silanol, iron(II) bromide (AnhydroBeads™, 99.999% trace metals basis), trimethylamine *N*-oxide and pyridine *N*-oxide were purchased from Sigma-Aldrich. Dioxygen was purchased from AirLiquide (99.99% purity with a water content < 1 ppm; No further treatment was applied). Soluble iodosobenzene was synthesized using the procedure of Protasiewicz *et al.*[28] under consideration of the safety precaution by Nguyen *et al.*[29]

General procedures: All experiments were carried out in an argon atmosphere using conventional Schlenk techniques or in glove boxes under argon or dinitrogen atmospheres with dioxygen and water concentrations below 1 ppm. Prior to use, glassware was heated under vacuum using a heat gun at 650 °C. Solvents were dried with a MBraun solvent purification system (SPS). THF was additionally and DME solely dried by distillation from Solvona®. Degassing was carried out by bubbling argon through the solvent for 30 min.

Analytical methods: **Elemental analysis** were carried out at a HEKO Euro 3000 elemental analyzer. **ESI MS** were obtained on an Agilent Technologies 6210 Time-of-Flight LC–MS instrument. **Mössbauer** data was collected on a SEECo MS6 spectrometer using a Rivertec MCo7.114 source. **ATR IR** spectra were recorded with a Bruker Alpha Fourier transform infrared spectrometer. **GC** analysis was carried out by using an AGILENT 7890B gas chromatograph (HP5 column, 30 m) with a flame-ionization detector coupled to an EI-MS AGILENT 5977B spectrometer with a triple-axis detector. The instrument was equipped with an autoinjector Agilent G4513 A (injection of approx. 10 µL; methods see SI). MS peaks were analyzed and compared with the library database of NIST MS Search 2.3. All EI-MS spectra of the detected peaks were in good agreement with the library database of the expected substances. **XRD** data collections were performed with a Bruker D8 Venture area detector with Mo–Kα radiation (λ = 0.71073 Å). Multi-scan absorption corrections implemented in Sadabs were applied to the data. The structures were solved by intrinsic phasing method (Shelxt-2014) and refined by full matrix least square procedures based on F^2 with all measured reflections (Shelxl-2018) with anisotropic temperature factors for all non-hydrogen atoms. All hydrogen atoms were added geometrically and refined by using a riding model.

Preparation of Ph_3SiONa, LNa: To a solution of NaH (86.8 mg, 3.61 mmol) (a previous report used NaOEt)[30] in thf (30 mL) a solution of triphenylsilanol, LH (1.00 g, 3.61 mmol, 1.0 equiv.) in thf (10 mL) was added dropwise via a syringe. The solution was stirred at room temperature for 3 h until evolution of gas had ceased. The resulting pale yellow solution was filtered and all volatiles were removed under vacuum. The resulting white solid was further dried by condensation of liquid argon (ca. 5 mL) into the flask and subsequently removing all volatiles under vacuum with vigorous stirring. LNa (1.01 g, 3.38 mmol, 94% yield) was obtained as a white powder. **^{1}H NMR** (300 MHz, MeCN-d_3) δ [ppm] = 7.11–7.14 (m, 6 H, H_{Ar}), 7.20–7.23 (m, 3 H, H_{Ar}), 7.39–7.41 (m, 6 H, H_{Ar}). **ATR IR** $\tilde{\nu}$ [cm^{-1}] = 3062 (w), 3016 (w), 2993 (w), 2975 (w), 1883 (w), 1822 (w), 1771 (w), 1586 (w), 1482 (w), 1425 (w), 1182 (w), 1103 (s), 1048 (m), 988 (s), 738 (m), 698 (s), 515 (s).

Synthesis of [Na(DME)][Fe_2L_5], **1**: To a solution of $FeBr_2$ (289 mg, 1.34 mmol) in dme (10 mL) a solution of LNa (1.00 g, 3.35 mmol, 2.5 equiv.) in dme (10 mL) was added. The resulting pale orange suspension was stirred for 3 h at room temperature. All volatiles were removed under vacuum with a water bath at 70 °C. The residue was dissolved in toluene (3 mL), filtered and layered with *n*-hexane (10 mL) for crystallisation. Single crystals of **1** (837 mg, 0.522 mmol, 78% yield), which were suitable for X-ray diffraction analysis, were obtained as reddish-brown needles after 10 days. **ATR IR** $\tilde{\nu}$ [cm^{-1}] = 3066 (w), 3047 (w), 2997 (w), 2940 (w), 2076 (w), 2043 (w), 2016 (w), 1981 (w), 1892 (w), 1825 (w), 1661 (w), 1588 (w), 1567 (w), 1483 (w), 1454 (w), 1426 (m), 1366 (w), 1332 (w), 1304 (w), 1260 (w), 1186 (w), 1156 (w), 1109 (s), 1074 (m), 1032 (m), 1019 (m), 995 (m), 943 (m), 868 (m), 740 (m), 695 (s), 566 (w), 505 (s). **ESI MS**

(MeCN, –MS): m/z = 1156.34 $[FeL_4]^-$ (calcd. 1156.29). **Mössbauer** Fe2: δ = 0.77 mm/s, ΔE_Q = 1.02; Fe1: δ = 1.07 mm/s, ΔE_Q = 2.40 mm/s. **Elemental analysis** calculated for $C_{94}H_{85}Fe_2NaO_7Si_5$ · toluene (1693.95 g/mol): C 71.61, H 5.53, found: C 71.60, H 5.51.

Synthesis of [Na(DME)][FeL$_3$], 2: To a solution of $FeBr_2$ (239 mg, 1.11 mmol) in dme (10 mL) a solution of LNa (1.00 g, 3.35 mmol, 3.0 equiv.) in dme (10 mL) was added. The resulting pale blue suspension was stirred for 2 h at room temperature. All volatiles were removed under vacuum. The residue was dissolved in toluene (3 mL), filtered and layered with *n*-hexane (10 mL) for crystallisation. Single crystals of **2** (950 mg, 0.954 mmol, 86% yield), which were suitable for X-ray diffraction analysis, were obtained as pale blueish-green needles after 4 days. **ATR IR** $\tilde{\nu}$ [cm^{-1}] = 3065 (w), 2996 (w), 2169 (w), 1964 (w), 1889 (w), 1824 (w), 1588 (w), 1566 (w), 1483 (w), 1448 (w), 1426 (s), 1304 (w), 1259 (w), 1189 (w), 1158 (w), 1110 (s), 1077 (m), 1040 (m), 1025 (m), 982 (m), 945 (s), 862 (w), 742 (s), 609 (s), 559 (m), 503 (s). **ESI MS** (MeCN, –MS): m/z = 1156.35 $[FeL_4]^-$ (calcd. 1156.29). **Mössbauer** Fe2: δ = 0.74 mm/s, ΔE_Q = 0.95. **Elemental analysis** calculated for $C_{58}H_{55}FeNaO_5Si_3$ (995.16 g/mol): C 70.00, H 5.57, found: C 69.75, H 5.50

Synthesis of [Na(DME)]$_2$[FeL$_4$], 3 and [Na(THF)]$_2$[FeL$_4$], 3-THF: To a solution of LNa (1.00 g, 3.35 mmol, 4.0 equiv.) in dme (**3**) or thf (**3-THF**) (10 mL) a solution of $FeBr_2$ (180 mg, 0.837 mmol) in dme (**3**) or thf (**3-THF**) (10 mL) was added. The resulting pale green suspension was stirred for 4 h at room temperature. All volatiles were removed under vacuum. The residue was dissolved in toluene (3 mL), filtered and layered with *n*-hexane (10 mL) for crystallisation. Single crystals of **3** (961 mg, 0.694 mmol, 83% yield) and **3-THF** (913 mg, 0.677 mmol, 81% yield), which were suitable for X-ray diffraction analysis, were obtained as pale green blocks after 7 days. **3**: **ATR IR** $\tilde{\nu}$ [cm^{-1}] = 3065 (w), 3044 (w), 3019 (w), 2937 (w), 2829 (w), 2179 (w), 1964 (w), 1891 (w),1827 (w), 1775 (w), 1587 (w), 1566 (w), 1482 (w), 1448 (w), 1426 (m), 1369 (w), 1187 (w), 1105 (s), 1078 (m), 957 (s), 740 (m), 700 (s), 524(s), 509 (s). **ESI MS** (MeOH, +MS): m/z = 1202.25 $[Na2FeL_4]^-$ (calcd. 1202.27). **Mössbauer** Fe2: δ = 1.16 mm/s, ΔE_Q = 2.66. **Elemental analysis** calculated for $C_{80}H_{80}FeNa_2O_8Si_4$ (1383,68 g/mol): C 69.44, H 5.83, found: C 69.24, H 5.85. **3-THF: ATR IR** $\tilde{\nu}$ [cm^{-1}] = 3065 (w), 2877 (w), 1483 (m), 1427 (w), 1185 (m), 1108 (m), 1043 (m), 983 (m), 740 (m), 607 (s), 506 (s), 429 (m). **ESI MS** (MeOH, +MS): m/z = 1202.25 $[Na_2FeL_4]^-$ (calcd. 1202.27). **Mössbauer** Fe2: δ = 1.13 mm/s, ΔE_Q = 2.51. **Elemental analysis** calculated for $C_{80}H_{76}FeNa_2O_6Si4$ (1347,65 g/mol): C 71.30, H 5.68, found: C 71.06, H 5.70.

Synthesis of [Na(DME)$_3$][FeL$_4$], 4: To a pale blueish-green solution of **2** (50 mg, 0.05 mmol) in toluene (3 mL) a solution of Me_3NO (3.77 mg, 0.05 mmol, 1 equiv.) in toluene (1 mL) was added. The stirred solution turned brown in an instant and after 30 s a colourless precipitate started to form. The supernatant was removed with a syringe and the residue was dissolved in toluene (8 mL). After filtration the pale-yellow solution was stored at 4 °C and colourless single crystals of **4** (23.2 mg, 0.016 mmol, 32% yield), suitable for X-ray diffraction analysis, were obtained after 2 weeks. **Elemental analysis** values did not fit well due to a brown precipitate which was not separatable from the crystals of **4**, **Mössbauer** δ = 0.34 mm/s, ΔE_Q = 0.44 mm/s.

Cyclohexene oxidation: 2 (20 mg, 0.02 mmol) was dissolved in cyclohexene (1 mL) and O_2 was bubbled through the solution for 20 s. The reaction was stirred for 16 h at room temperature and biphenyl (3.09 mg, 0.02 mmol, 1 equiv.) was added as a standard. After the addition of C_6D_6 (1 ml) the reaction mixture was filtered through celite® and cyclohexene oxidation products were analysed with GC MS and NMR.

Deposition Numbers 2124123 (for **1xC_7H_8**), 2124124 (for **2**), 2124125 (for **3-THF**) and 2124125 (for **4**) contain the supplementary crystallographic data for this paper. These data are provided free of charge by the joint Cambridge Crystallographic Data Centre and Fachinformationszentrum Karlsruhe Access Structures service www.ccdc.cam.ac.uk/structures.

Acknowledgements

We are grateful to the Deutsche Forschungsgemeinschaft (LI-714 12-1) and the Humboldt-Universität zu Berlin for financial support. For the support with GC measurements and the fruitful discussions we would like to thank Dustin Kass. Open Access funding enabled and organized by Projekt DEAL.

Conflict of Interest

The authors declare no conflict of interest.

Data Availability Statement

The data that support the findings of this study are available in the supplementary material of this article.

Keywords: Cyclohexene · Iron · O atom transfer · Oxidation · Siloxide · Structure

[1] S. Yelin, C. Limberg, *Catal. Lett.* **2020**, *150*, 1–11.
[2] D. Pinkert, C. Limberg, *Chem. Eur. J.* **2014**, *20*, 9166–9175.
[3] G. I. Panov, V. I. Sobolev, A. S. Kharitonov, *J. Mol. Catal.* **1990**, *61*, 85–97.
[4] B. E. R. Snyder, P. Vanelderen, M. L. Bols, S. D. Hallaert, L. H. Böttger, L. Ungur, K. Pierloot, R. A. Schoonheydt, B. F. Sels, E. I. Solomon, *Nature* **2016**, *536*, 317–321.
[5] B. E. R. Snyder, M. L. Bols, R. A. Schoonheydt, B. F. Sels, E. I. Solomon, *Chem. Rev.* **2018**, *118*, 2718–2768.
[6] C. Nozaki, C. G. Lugmair, A. T. Bell, T. D. Tilley, *J. Am. Chem. Soc.* **2002**, *124*, 13194–13203.
[7] R. Duchateau, *Chem. Rev.* **2002**, *102*, 3525–3542; V. Lorenz, F. T. Edelmann, *Adv. Organomet. Chem.* **2005**, *53*, 101–153; C. Copéret, M. Chabanas, R. Petroff Saint-Arroman, J.-M. Basset, *Angew. Chem. Int. Ed.* **2003**, *42*, 156–181; *Angew. Chem.* **2003**, *115*, 164–191; R. W. J. M. Hanssen, R. A. van Santen, H. C. L. Abbenhuis, *Eur. J. Inorg. Chem.* **2004**, 675–683; E. A. Quadrelli, J.-M. Basset, *Coord. Chem. Rev.* **2010**, *254*, 707–728; F. J. Feher, T. A. Budzichowski, *Polyhedron* **1995**, *14*, 3239–3253.
[8] N. Manicke, S. Hoof, M. Keck, B. Braun-Cula, M. Feist, C. Limberg, *Inorg. Chem.* **2017**, *56*, 8554–8561.
[9] D. Pinkert, M. Keck, S. G. Tabrizi, C. Herwig, F. Beckmann, B. Braun-Cula, M. Kaupp, C. Limberg, *Chem. Commun.* **2017**, *53*, 8081–8084.
[10] D. Pinkert, S. Demeshko, F. Schax, B. Braun, F. Meyer, C. Limberg, *Angew. Chem. Int. Ed.* **2013**, *52*, 5155–5158; *Angew. Chem.* **2013**, *125*, 5260–5263.
[11] F. Beckmann, D. Kass, M. Keck, S. Yelin, S. Hoof, B. Cula, C. Herwig, K. B. Krause, D. Ar, C. Limberg, *Z. Anorg. Allg. Chem.* **2021**, *647*, 960–967.
[12] K. Warm, G. Tripodi, E. Andris, S. Mebs, U. Kuhlmann, H. Dau, P. Hildebrandt, J. Roithová, K. Ray, *Angew. Chem. Int. Ed.* **2021**, *60*, 23018–23024.
[13] M. B. Chambers, S. Groysman, D. Villagrán, D. G. Nocera, *Inorg. Chem.* **2013**, *52*, 3159–3169.
[14] A. N. Kornev, T. A. Chesnokova, V. V. Semenov, E. V. Zhezlova, L. N. Zakharov, L. G. Klapshina, G. A. Domrachev, V. S. Rusakov, *J. Organomet. Chem.* **1997**, *547*, 113–119.

Research Article
doi.org/10.1002/ejic.202200078

[15] P. Šot, M. A. Newton, D. Baabe, M. D. Walter, A. P. Bavel, A. D. Horton, C. Copéret, J. A. Bokhoven, *Chem. Eur. J.* **2020**, *26*, 8012–8016.
[16] P. Gütlich, E. Bill, A. X. Trautwein, *Mössbauer Spectroscopy and Transition Metal Chemistry*, Springer-Verlag Berlin Heidelberg, Berlin Heidelberg, **2011**.
[17] Y. Sanakis, P. P. Power, A. Stubna, E. Münck, *Inorg. Chem.* **2002**, *41*, 2690–2696.
[18] D. J. Evans, D. L. Hughes, J. Silver, *Inorg. Chem.* **1997**, *36*, 747–748.
[19] E. Murad, J. Cashion, *Mössbauer Spectroscopy of Environmental Materials and Their Industrial Utilization*, Springer US, Boston, **2004**.
[20] J. Hohenberger, K. Ray, K. Meyer, *Nat. Commun.* **2012**, *3*, 720.
[21] J. Park, Y. Morimoto, Y.-M. Lee, W. Nam, S. Fukuzumi, *Inorg. Chem.* **2014**, *53*, 3618–3628.
[22] X. Engelmann, D. D. Malik, T. Corona, K. Warm, E. R. Farquhar, M. Swart, W. Nam, K. Ray, *Angew. Chem. Int. Ed.* **2019**, *58*, 4012–4016; *Angew. Chem.* **2019**, *131*, 4052–4056.
[23] W. Nam, *Acc. Chem. Res.* **2007**, *40*, 522–531.
[24] D. Ar, A. F. R. Kilpatrick, B. Cula, C. Herwig, C. Limberg, *Inorg. Chem.* **2021**, *60*, 13844–13853.
[25] Y. N. Wei, H. Li, F. Yue, Q. Xu, J. D. Wang, Y. Zhang, *RSC Adv.* **2016**, *6*, 107104–107108.
[26] I. M. Denekamp, M. Antens, T. K. Slot, G. Rothenberg, *ChemCatChem* **2018**, *10*, 1035–1041.
[27] J. Büker, B. Alkan, Q. Fu, W. Xia, J. Schulwitz, D. Waffel, T. Falk, C. Schulz, H. Wiggers, M. Muhler, B. Peng, *Catal. Sci. Technol.* **2020**, *10*, 5196–5206.
[28] D. Macikenas, E. Skrzypczak-Jankun, J. D. Protasiewicz, *J. Am. Chem. Soc.* **1999**, *121*, 7164–7165.
[29] J. T. Hopp, S. T. Nguyen, *C&EN* **2011**, *89*, 2.
[30] P. Wytrych, J. Utko, J. Klak, M. Ptak, M. Stefanski, T. Lis, J. Ejfler, L. John, *Molecules* **2022**, *27*, 147.

Manuscript received: February 3, 2022
Revised manuscript received: March 14, 2022
Accepted manuscript online: March 17, 2022